

Effects of MnO on the Dissolution Behavior of Lime in CaO–SiO₂–FeO–P₂O₅–MnO Slag



GUILIN SUN, XINYU LI, YUNJIN XIA, JIE LI, and DINGDONG FAN

In this study, the effects of MnO on the dissolution behavior of lime in CaO–SiO₂–FeO–P₂O₅–MnO slag were explored. After the lime is immersion in the slag, four regions are formed around the surface: unmelted calcium oxide, a discontinuous CaO–FeO (MnO) layer, a dense layer containing chemical compounds and solid solution, and original slag. The dense layer composed of C₃S, C₂S, and C₂S–C₃P can hinder the lime dissolution and the thickness of this layer depends on the MnO content and immersion time. The average lime dissolution rate is improved slightly when the MnO content changes from 0 to 3 pct, and it increases significantly with a further increase in MnO content. The effects of MnO on the lime dissolution are discussed based on the phase diagram and viscosity calculation.

<https://doi.org/10.1007/s11663-023-02805-5>

© The Minerals, Metals & Materials Society and ASM International 2023

I. INTRODUCTION

LIME is one of the main fluxes in steelmaking. The fast and complete dissolution of lime in slag can increase the reaction rate of dephosphorization and reduce slag consumption and free calcium oxide content. Therefore, many research studies have been conducted to investigate the dissolution mechanism of lime in steelmaking slag under static and dynamic conditions.^[1–17]

Umakoshi *et al.*^[1] studied the dissolution rate of burnt dolomite in molten FeO–CaO–SiO₂ slags as a function of temperature and rotational speed and found that the formation of 2CaO·SiO₂ film hindered the dissolution of CaO. Amini *et al.*^[2] investigated the lime dissolution in molten slags under static conditions and verified that the 2CaO·SiO₂ layer affected the dissolution rate. Deng *et al.*^[3] studied the dissolution of lime in synthetic FeO–SiO₂ and CaO–FeO–SiO₂ slags in a closed tube furnace at 1873 K and revealed that a dense layer of 2CaO·SiO₂ could hinder the dissolution. Further investigation under forced convection showed that the main mechanism of lime dissolution was through removal of the interface layer(s) including 2CaO·SiO₂ by shear stress.^[4] Sun *et al.*^[5,6] observed the dissolution behavior of solid lime particles in liquid slags at high

temperatures using confocal scanning laser microscopy and found that the formation of an interfacial reaction layer affected the dissolution rate.

The dissolution behavior of lime is related to the properties of the slag and the lime. Yang *et al.*^[7] and Vieira *et al.*^[8] assessed the effect of lime particle size on the melting behavior of lime-containing fluxes and showed that decreasing the lime particle size could promote the dissolution of lime in both CaO–SiO₂–FeO and CaO–Al₂O₃–FeO slags. Natalie and Evans^[9] studied the relationship between lime properties and the rate of dissolution in molten slags and concluded that reactive and porous lime tended to dissolve rapidly in the slag. Maruoka *et al.*^[10,11] measured the dissolution rates of dense lime and metallurgical lime in CaO–SiO₂–FeO, CaO–Al₂O₃–FeO, and CaO–B₂O₃–FeO slags and found that the porosity of lime had limited impact on the dissolution rate after the formation of the reaction layer. They also reported that the dissolution rate of metallurgical lime was faster than that of dense and porous lime owing to the generation of internal gas. The effect of CO₂ content in quicklime on dissolution rate was further investigated in steelmaking slags and the significantly enhanced dissolution rate was related to the gases generated *via* the thermal decomposition of residual limestone.^[12–14] Martinsson *et al.*^[15] studied the dissolution mechanisms of lime in liquid and foaming slags from the basic oxygen furnace (BOF) process. Two different slags with FeO contents of 45 and 25 wt pct were used to represent the early and later stages of the converter process, respectively. The controlling mechanism of lime dissolution in liquid slag was the removal of the 2CaO·SiO₂ layer, while the controlling mechanism in foaming slag was the contact area between the lime and the liquid phase of the foam.

GUILIN SUN, XINYU LI, YUNJIN XIA, JIE LI, and DINGDONG FAN are with the School of Metallurgical Engineering, Anhui University of Technology, Ma'anshan 243002, Anhui, P.R. China. Contact e-mail: xyjssss@aliyun.com

Manuscript submitted November 30, 2022; accepted April 15, 2023.

Article published online May 8, 2023.

The compositions of actual steelmaking slag are complex and usually contain P_2O_5 , MgO , *etc.*, which inevitably affect the lime dissolution process. Li *et al.*^[16] studied the dissolution of lime in basic oxygen steel (BOS) slag and showed that a $2CaO\cdot SiO_2\text{--}3CaO\cdot P_2O_5$ solid solution layer, instead of a $2CaO\cdot SiO_2$ layer, was formed in an industrial converter. Kakimoto *et al.*,^[17] Kikuchi *et al.*^[18] and Cao *et al.*^[19] investigated the influence of P_2O_5 on the lime dissolution behavior and found that P_2O_5 accelerated the dissolution in the molten slag. Cheremisina *et al.*^[20] clarified the influence of the MgO content on the kinetics of lime dissolution in steelmaking slag and reported that the solubility of lime decreased with increasing MgO content owing to the formation of high-temperature solid compounds ($2CaO\cdot SiO_2$ and $(Mg,Fe)_2SiO_4$) and solutions.

In recent years, a ‘Double Slag + Slag Remaining’ process with direct alloying of manganese ore has been used in the BOF steelmaking process in China to lower production cost, while decarburization slag with high MnO content is recycled to reduce slag generation.^[21–25] This process increases the MnO content in the slag and possibly affect the dissolution of lime, particularly in the early stages of the BOF steelmaking process. There has been no systematic research on the influence of MnO content on lime dissolution in the BOF steelmaking process. Therefore, this study investigated the dissolution behavior of lime in $CaO\text{--}SiO_2\text{--}FeO\text{--}P_2O_5\text{--}MnO$ slags with different MnO contents.

II. EXPERIMENT

A. Sample Preparation

Cylindrical lime samples with a radius of 10 mm and a height of 40 mm were obtained by pressuring CaO powder in a mold for 120 seconds using an oil hydraulic press under a pressure of 50 MPa pressure. The porosity of the lime samples was approximately 60 pct. The lime samples were then sintered and activated at 1000 °C for 6 hours in a silicon molybdenum bar-resistance furnace.

According to the formulation in Table I, a mixed oxide of $CaO\text{--}SiO_2\text{--}FeO\text{--}P_2O_5\text{--}MnO$ was prepared by mixing reagent-grade SiO_2 , MnO , $3CaO\cdot P_2O_5$, $C_2FeO_4\cdot 2H_2O$, and synthesized CaO (calcined the reagent-grade $CaCO_3$ at 1100 °C for 6 hours).

Table I. Chemical Compositions of Slag (Weight Percent)

| No. | CaO | SiO ₂ | FeO | P ₂ O ₅ | MnO |
|-----|-------|------------------|-------|-------------------------------|-------|
| 1 | 45.00 | 30.00 | 20.00 | 5.00 | 0 |
| 2 | 43.20 | 28.80 | 20.00 | 5.00 | 3.00 |
| 3 | 42.00 | 28.00 | 20.00 | 5.00 | 5.00 |
| 4 | 40.80 | 27.20 | 20.00 | 5.00 | 7.00 |
| 5 | 39.00 | 26.00 | 20.00 | 5.00 | 10.00 |

B. Dissolution Experiments and Characterization

The mixed oxide (100 g) was placed in a pure iron crucible (80 mm height and 50 mm outside diameter) with an Al_2O_3 crucible (150 mm height and 110 mm diameter), and then melted at $1\ 673 \pm 5\ K$ ($1400 \pm 5\ ^\circ C$) for 30 minutes in a silicon molybdenum bar-resistance furnace with Ar gas protection. After completely melted, the prepared cylindrical lime sample fixed at the end of a molybdenum rod was hung approximately 2 cm above the iron crucible and preheated for 5 minutes to prevent lime breakage due to rapid temperature increase after it contacted the slag. The preheated lime was immersed in the slag and hold for 10, 60, 120, and 1000 seconds, respectively, and then removed from the slag quickly and cooled to room temperature with injected Ar gas. A schematic of the silicon molybdenum bar-resistance furnace is shown in Figure 1. To reduce the experimental error, dissolution experiments at different times were carried out independently. The bulk composition of the slag was analyzed using X-ray fluorescence (XRF). The phase components of the reaction product on the lime surface were determined using X-ray diffraction (XRD). The cross-sectional areas of the cooled samples were observed by scanning electron microscopy (SEM), and the compositions at various positions on the lime surface were determined using energy-dispersive spectroscopy (EDS). Because the EDS analysis was not very accurate, most of the EDS analysis results were used as a tool for discussions.

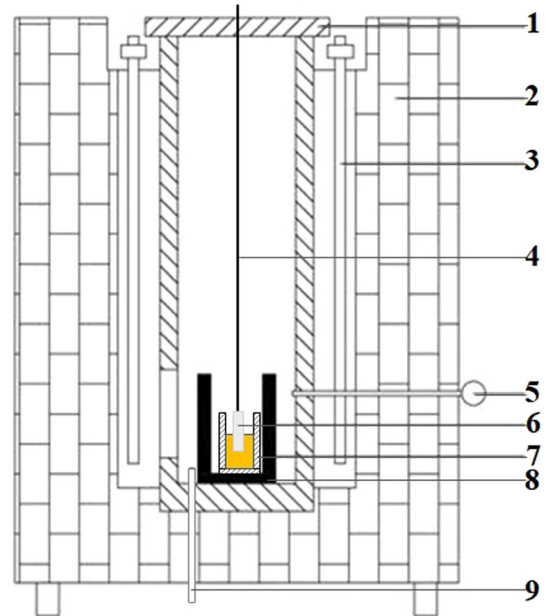


Fig. 1—Schematic of the silicon molybdenum bar-resistance furnace. 1—Cover; 2—Furnace stack; 3—Silicon molybdenum bar; 4—Mo wire; 5—Thermocouple (PtRh6–PtRh30); 6—Lime; 7—Pure iron crucible; 8— Al_2O_3 crucible; 9—Ar tube.

III. RESULTS

A. Phase Transition During the Dissolution Process

Figure 2 shows the SEM images of the reaction interface of lime in slag 2 at different times and Figure 3 displays the EDS results of the positions labeled in the SEM images. As shown in Figure 2, four regions are identified around the lime surface. Region A mainly consisting of CaO at position 1 is related to unmelted calcium oxide, while region B with a large amount of CaO and FeO, and a small amount of MnO at position 2 corresponds to the CaO–FeO (MnO) layer. Region C contains Ca, Si, and P, corresponding to chemical compounds and solid solutions, and region D is the original slag. The CaO–FeO (MnO) layer, as shown in Figures 2(c) and (d), is discontinuous, and the thickness of the layer changes slightly with increasing immersion time. In contrast, the solid compound and solution layer are much denser, and its thickness increases with the increase in immersion time.

To precisely determine the phase components during the dissolution process, the reaction products on the lime surface were analyzed using XRD. As shown in Figure 4, the reaction product is composed of $3\text{CaO}\cdot\text{SiO}_2$ (C_3S), $2\text{CaO}\cdot\text{SiO}_2$ (C_2S), $2\text{CaO}\cdot\text{SiO}_2\text{-}3\text{CaO}\cdot\text{P}_2\text{O}_5$ ($\text{C}_2\text{S-C}_3\text{P}$), $\text{Ca}_2\text{Fe}_2\text{O}_4$, $\text{Mn}_2\text{Fe}_2\text{O}_4$, and FeO phases. According to the EDS results in Figure 3, region B mainly contains Ca and Fe; therefore, the

main phases of region B are $\text{Ca}_2\text{Fe}_2\text{O}_4$ and $\text{Mn}_2\text{Fe}_2\text{O}_4$. In region C, the Ca content decreases and Si content increases from the lime surface to the bulk slag. The molar ratio of CaO/SiO_2 is approximately 3 near the lime surface and decreases to 2 near the slag. As a result, the phases of region C may transit from C_3S (closed to region B), C_2S (in the middle of region C) to $\text{C}_2\text{S-C}_3\text{P}$ (close to region D).

Figure 5 shows the positions of the average compositions of different regions in the CaO–SiO₂–FeO–MnO phase diagram at 1400 °C and 1 atm. The average compositions of regions A, B, C, and D are distinguished by blue, yellow, green, and black, respectively, and immersion times of 10, 60, 120, and 1000 seconds are represented by circles, triangles, squares, and diamonds, respectively. The average composition analysis was measured by EDS for regions A, B, and C. The composition of region D (bulk slag) was analyzed by XRF because the precipitation of the gray $\text{C}_2\text{S-C}_3\text{P}$ phase and white RO phases ($\text{Ca}_2\text{Fe}_2\text{O}_4$, $\text{Mn}_2\text{Fe}_2\text{O}_4$, or FeO) can affect the accuracy of the EDS analysis. As shown in Figure 5, the average composition of region A is near the CaO corner at the CaO–FeO line in the phase diagram and remains unchanged with immersion time. This indicates that Ca^{2+} can transfer quickly from region A to region B. The average composition of region B after an immersion time of 10 seconds is near the liquidus in the L + CaO region, and it moves to the

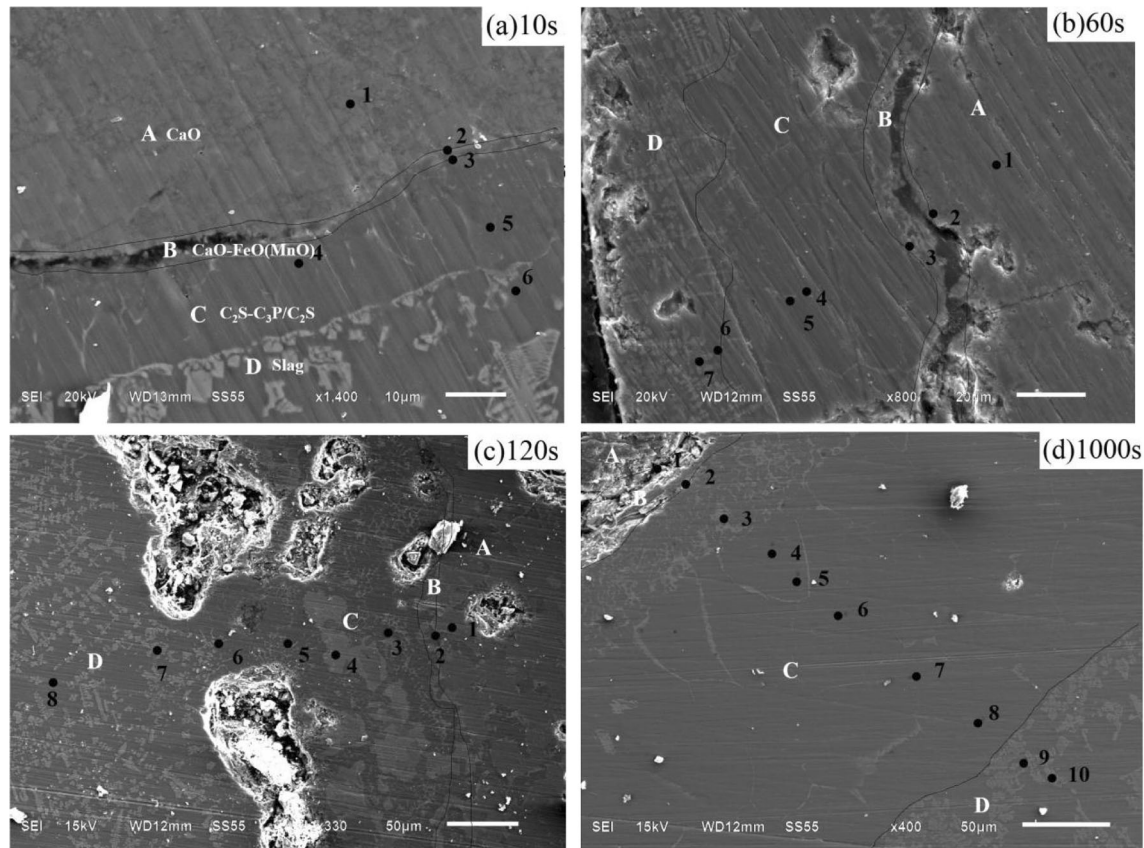


Fig. 2—SEM images of the interface of lime dissolution in slag 2 after different reaction times (a) immersion time of 10 seconds, (b) immersion time of 60 seconds, (c) immersion time of 120 seconds, (d) immersion time of 1000 seconds.

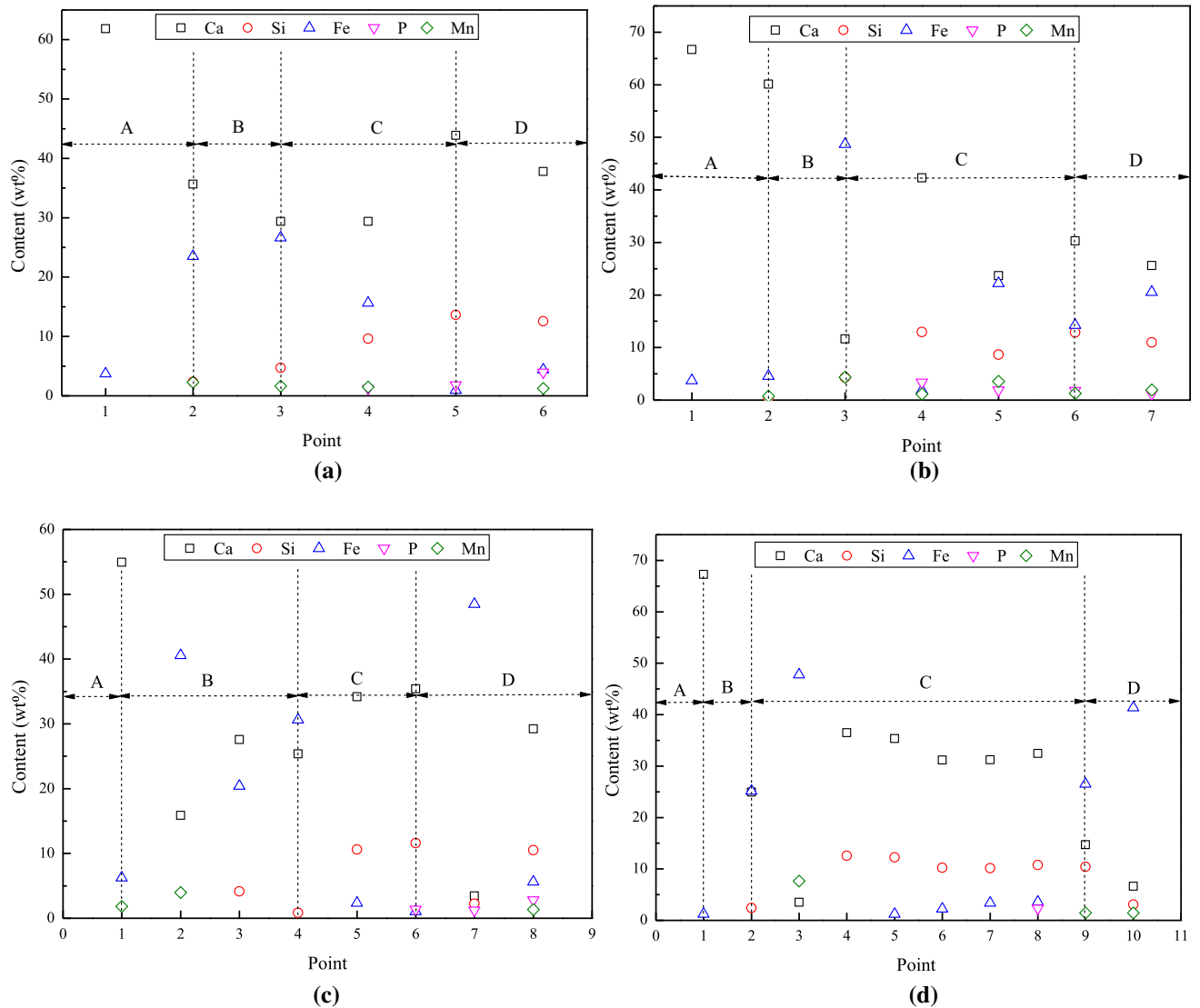


Fig. 3—Slag compositions of different points in regions A (a), B (b), C (c), and D (d) in Fig. 2 analyzed by EDS.

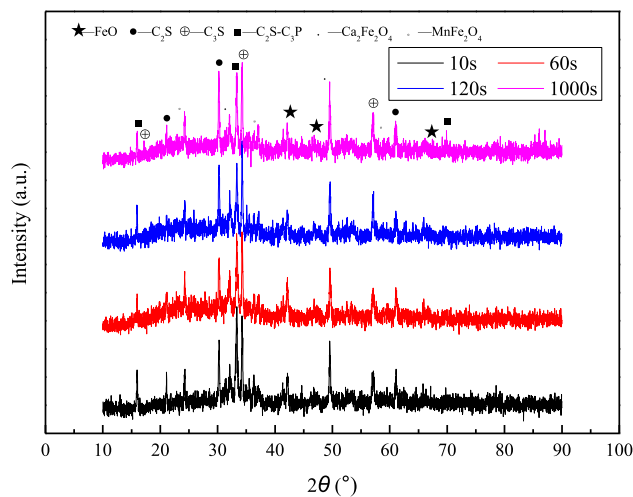


Fig. 4—XRD patterns of the reaction products on the lime surface.

liquid region with increasing immersion time. Because the average compositions of region B are almost located in the liquid region, the easy mass transfer of Ca^{2+} and Fe^{2+} makes region B discontinuous. The average composition of region C is in the $L + C_2S + C_3S$ region and moves from near the saturation curve of the $L + C_2S + C_3S$ region to the saturation curve of the $L + C_3S + CaO$ region. This shows that the mass transfer of Ca^{2+} in region C is slow, leading to the accumulation of CaO. The average composition of region D is in the $L + C_2S$ region, and the CaO content increases gradually with increasing immersion time. Because the average compositions of regions B and D are almost in the liquid region, and the accumulation of CaO is only found in region C. Therefore, the mass transfer of Ca^{2+} and Fe^{2+} in regions A, B, and D is significantly faster than that in region C, this suggests that the formation of solid compound and solution layer in region C hinders the dissolution, consistent with the research works of Umakoshi *et al.*^[1] and Amini *et al.*^[2]

B. Effect of MnO Content on Dissolution Rate

Figure 6 shows the correlation between average dissolution rate (expressed by the reduction in the lime sectional area within 1000 seconds) and the MnO content in the slag. The average dissolution rate increases slowly with an increase in MnO content from 0 to 3 pct. However, with a further increase in the MnO content, the average dissolution rate increases significantly. The lime dissolution rate in slag 5 (10 pct of MnO) is about 1.43 times higher than that of slag 1 (0 pct of MnO). This indicates that MnO can prompt the dissolution when its content is higher than 3 pct and the prompting effect is limited when MnO content is less than 3 pct.

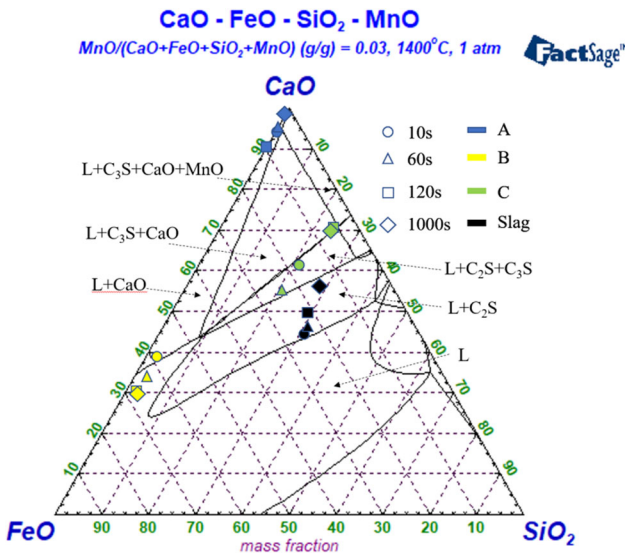


Fig. 5—Positions of the average compositions of different regions after lime immersion for different times in CaO–SiO₂–FeO–MnO phase diagram at 1400 °C and 1 atm (Color figure online).

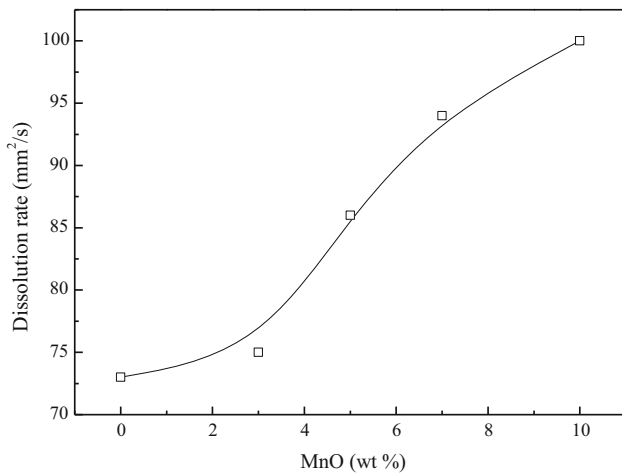


Fig. 6—Variation of average dissolution rate of lime with MnO content in slag.

C. Effect of MnO Content on the Average Thickness of Solid Compound and Solution Layer

Figure 7 shows the effect of immersion time on the average thickness of the solid compound and solution layer for slags with different MnO contents. The thicknesses were obtained by analyzing the SEM images using Image J software. As the CaO–FeO (MnO) layer is discontinuous and difficult to measure accurately, only the average thickness of the dense solid compound and solution layer was obtained. As shown in Figure 7, the thickness of the solid compound and solution layer increases gradually with increasing immersion time for each slag. However, the influence of MnO content also depends on the immersion time. When the immersion time was short (10 seconds), the effect of the MnO content on the thicknesses of the solid compound and solution layer was insignificant. However, with the increase in immersion time, the variation in MnO content can considerably affect the thickness of the solid compound and solution layer. The thickness difference between slags with different MnO contents becomes more significant when the immersion time is extended.

IV. DISCUSSION

A. Dissolution Process of Lime in CaO–SiO₂–FeO–P₂O₅–MnO Slag

Figure 8 shows a schematic diagram of lime dissolution in CaO–SiO₂–FeO–P₂O₅–MnO slag. The dissolution process of lime can be described as follows.

After the lime is immersed in the slag, under the drive of a concentration gradient, Ca²⁺ ions in the lime diffuse into the slag and Fe²⁺, Mn²⁺, PO₄³⁻, and SiO₃²⁻ ions in the slag diffuse into the lime. Because the radii of Fe²⁺ and Mn²⁺ ions are much smaller than those of PO₄³⁻ and SiO₃²⁻ ions, Fe²⁺ and Mn²⁺ ions can transfer quickly from the slag to lime and react with the lime to form a CaO–FeO (MnO) layer near the

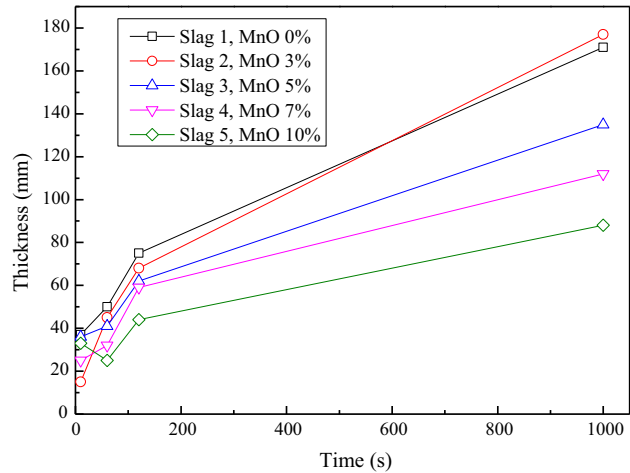


Fig. 7—Effect of immersion time on the average thickness of solid compound and solution layer.

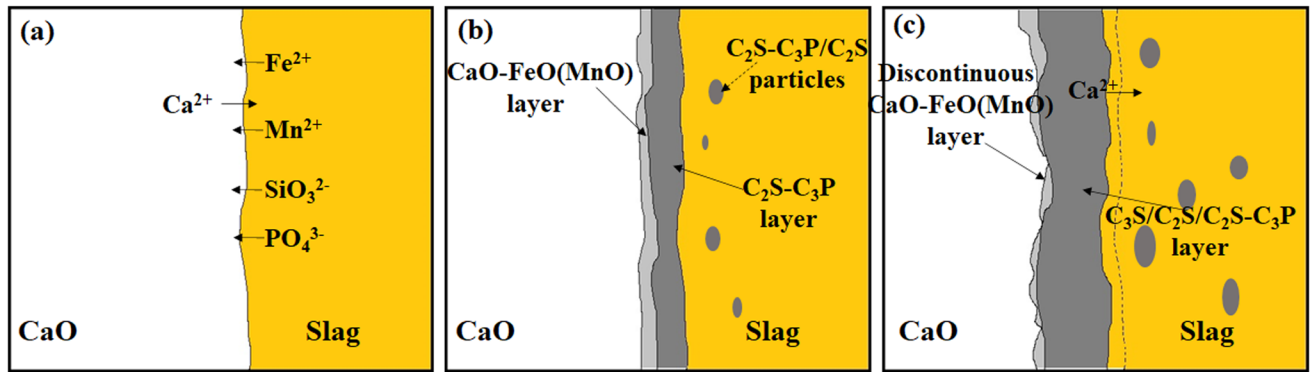


Fig. 8—Schematic of lime dissolution in CaO-SiO₂-FeO-P₂O₅-MnO slag (a) diffusion of ions (b) formation of different layers, (c) changing of different layers.

surface. PO₄³⁻ and SiO₃²⁻ with larger ionic radii diffuse slowly and react with Ca²⁺ diffused from the lime to form a C₂S-C₃P solid solution layer. Simultaneously, with an increase in the CaO content, the C₂S-C₃P solid solution or C₂S solid-phase precipitates from the bulk slag because the initial composition of the slag locates on the C₂S saturation line. With increasing immersion time, the fast mass transfer of Fe²⁺ and Mn²⁺ ions from the slag makes the CaO-FeO (MnO) layer discontinuous. The formation of solid compound and solution layer hinders the mass transfer of Ca²⁺ ions from lime to slag, causing CaO accumulate and generate C₃S solid phase. Because the formation rate of the solid compound and solution layer is much faster than the dissolution rate, the thickness of the solid compound and solution layer increases gradually. The removal of the solid compound and solution layer with forced convection in a BOF converter is crucial to promoting lime dissolution.

B. Effect of MnO on the Dissolution Path and Viscosity of Slag

Combining the lime dissolution process and MnO distribution in the slag, the effect of MnO content on the lime dissolution process may have two aspects. On the one hand, as shown in Figure 2, MnO can affect the dissolution path of lime and the composition of region B. Figure 9 shows the lime dissolution paths in CaO-SiO₂-FeO and CaO-SiO₂-FeO-MnO phase diagrams at 1400 °C. The direct dissolution paths indicated by the blue line in Figure 9 are used to analyze the lime dissolution process, although the actual dissolution paths may be more complex (Figure 5). Compared with the dissolution in the slag without MnO, a region containing C₃S and MnO is identified when the lime is dissolved in the slag containing MnO. This region is found at position 3 in Figure 2(d), where a discontinuous precipitate layer containing several C₃S crystals and a white phase with high MnO content are located near the solid compound and solution layer. The discontinuous precipitate layer can prompt the mass transfer of CaO from lime to slag. According to CaO-SiO₂-FeO-MnO phase diagram in Figure 9,

MnO crystals are supposed to precipitate together with C₃S. However, no MnO crystals were detected by SEM and XRD, possibly because the precipitated MnO reacts with FeO to form a compound, as shown in the XRD results (Figure 4).

Figure 10 shows the changes in the MnO content in region B with the MnO content in the slag. The MnO content in region B increases almost linearly with the increase in the MnO content in the slag. The increase in MnO content reduces the melting point of region B and expands the liquid-phase region according to the CaO-FeO-MnO phase diagram.^[26] The increase in liquid-phase ratio in region B induces a discontinuous CaO-FeO (MnO) layer, facilitating the mass transfer of Ca²⁺, Fe²⁺, and Mn²⁺ ions through the CaO-FeO (MnO) layer and accelerating the dissolution.

On the other hand, MnO as a basic oxide can change the viscosity of the slag, thereby impact the mass transfer of ions. To investigate the effect of MnO content on the viscosity, FactSage software was used to calculate the viscosity of the CaO-SiO₂-FeO-P₂O₅-MnO slag. Figure 11 shows the effect of the MnO content on the viscosity of the slag calculated by the FactSage software. The viscosity of the slag decreases almost linearly with increasing MnO content. The reduction in viscosity was conducive to the mass transfer of the solute in the slag, thus promoting the dissolution of lime. Because MnO can significantly affect the lime dissolution paths and change the viscosity of the slag, it can be sure that the increased lime dissolution rate is due to increased MnO, and not due to the decreased CaO in slag.

V. CONCLUSIONS

The effects of the MnO content on the dissolution behavior of lime in CaO-SiO₂-FeO-P₂O₅-MnO slag were studied. The results are summarized as follows:

- (1) When lime is immersed in CaO-SiO₂-FeO-P₂O₅-MnO slag, four regions are identified around the lime surface: unmelted CaO (region A), discontinuous CaO-FeO (MnO) layer (region B), dense

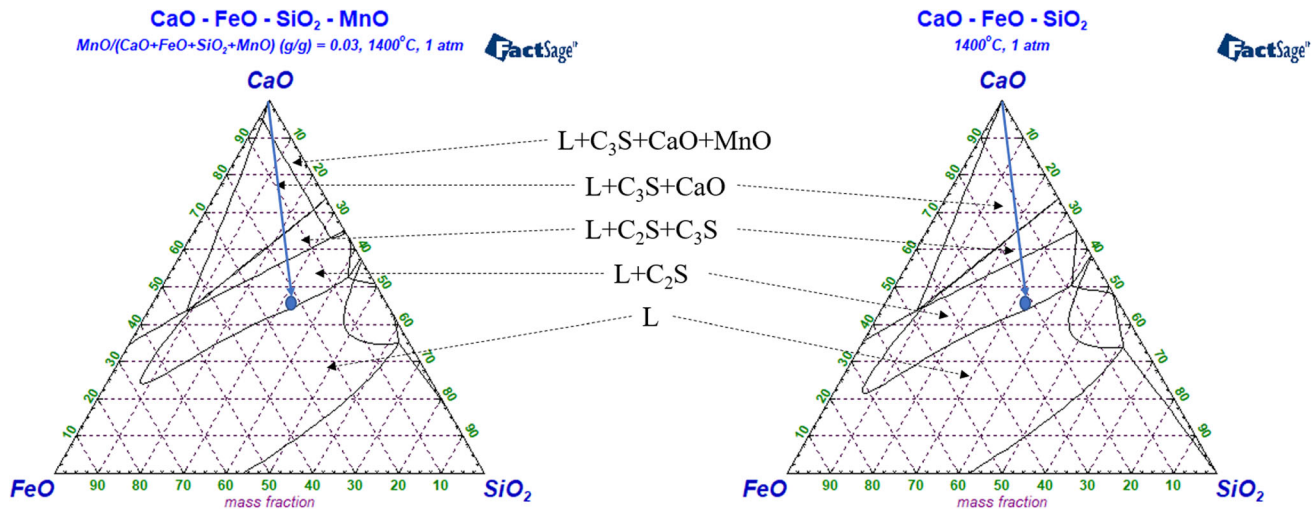


Fig. 9—Lime dissolution paths in CaO–SiO₂–FeO and CaO–SiO₂–FeO–MnO phase diagrams at 1400 °C.

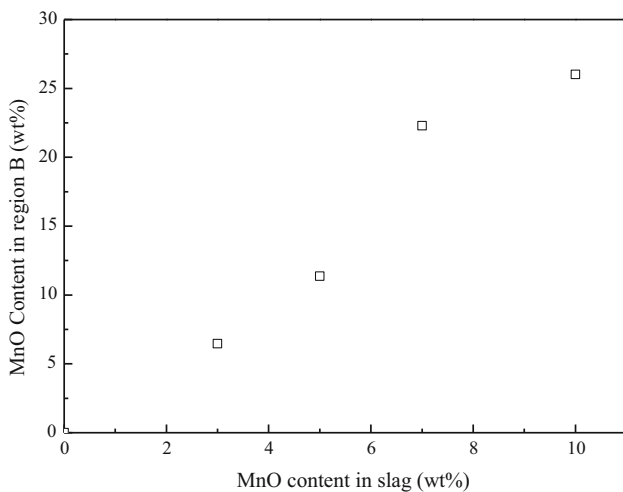


Fig. 10—Correlation between MnO contents in region B and in slag.

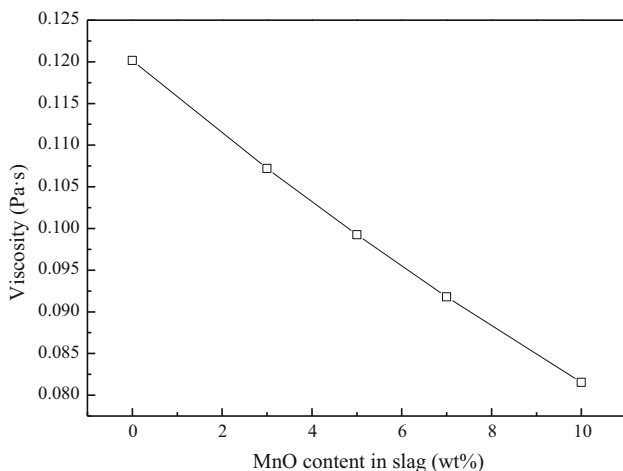


Fig. 11—Effect of MnO content on the viscosity of the slag calculated by the FactSage software.

- solid compound and solution layer (region C), and the original slag (region D).
- (2) In the phase diagram, the average composition of region A is near the CaO corner at the CaO–FeO line and does not change with immersion time. The average composition of region B moves from near the liquidus in the L + CaO region to the liquid region with the increasing immersion time, and the average composition of region C moves from near the saturation curve of the L + C₂S + C₃S region to the saturation curve of the L + C₃S + CaO region. The average composition of region D is in the L + C₂S region.
 - (3) The average dissolution rate is slightly increased when the MnO content changes from 0 to 3 pct, but increases significantly with a further increase in MnO content.
 - (4) A high MnO content in slag can affect the dissolution path of lime, increase the liquid-phase ratio in region B, and decrease the viscosity of the slag, thereby accelerating the dissolution of lime.

ACKNOWLEDGMENTS

The authors would like to express their gratitude to the National Natural Science Fund (Grant Nos. 52074001, 52074003, 52204329), the Anhui Provincial Natural Science Foundation (Grant No. 2108085QE215), and the Natural Science Foundation of Educational Department of Anhui Province (Grant Nos. KJ2020A0273, 2022AH010024) for sponsoring this study. We would like to thank Editage (www.editage.cn) for English language editing.

CONFLICT OF INTEREST

On behalf of all the authors, the corresponding author states that there is no conflict of interest.

REFERENCES

1. M. Umakoshi, M. Katsumi, and K. Yasuji: *Trans. ISIJ*, 1984, vol. 24, pp. 532–39.
2. S. Amini, B. Michael, and O. Oleg: *ISIJ Int.*, 2007, vol. 47, pp. 32–7.
3. T. Deng, J. Gran, and D. Sichen: *Steel Res. Int.*, 2010, vol. 81, pp. 347–55.
4. T. Deng and D. Sichen: *Metall. Mater. Trans. B*, 2012, vol. 43B, pp. 578–86.
5. Z.H.I. Sun, X. Guo, J.V. Dyck, M. Guo, and B. Blanpain: *AICHE J.*, 2013, vol. 59, pp. 2907–916.
6. X. Guo, Z.H.I. Sun, J.V. Dyck, M. Guo, and B. Blanpain: *Ind. Eng. Chem. Res.*, 2014, vol. 53, pp. 6325–333.
7. J. Yang, M. Kuwabara, T. Asano, A. Chuma, and J. Du: *ISIJ Int.*, 2007, vol. 47, pp. 1401–408.
8. L.M. Vieira, H.C.C. Oliveira, V.B. Telles, E. Junca, E.A. Vieira, and J.R. Oliveira: *J. Mater. Res. Technol.*, 2020, vol. 9, pp. 14878–4886.
9. C.A. Natalie and J.W. Evans: *Ironmak. Steelmak.*, 1979, vol. 6, pp. 101–09.
10. N. Maruoka, A. Ishikawa, H. Shibata, and S.Y. Kitamura: *High Temp. Mater. Process.*, 2013, vol. 32, pp. 15–24.
11. N. Maruoka, A. Ishikawa, H. Shibata, and S.Y. Kitamura: *CAMP-ISIJ*, 2012, vol. 25, pp. 217–20.
12. N. Maruoka and H. Nogami: *Metall. Mater. Trans. B*, 2017, vol. 48B, pp. 113–18.
13. N. Maruoka, A. Ito, M. Hayasaka, S.Y. Kitamura, and H. Nogami: *ISIJ Int.*, 2017, vol. 57, pp. 1677–683.
14. N. Maruoka, A. Ito, M. Hayasaka, and H. Nogami: *ISIJ Int.*, 2017, vol. 57, pp. 1684–690.
15. J. Martinsson, B. Glaser, and D. Sichen: *Metall. Mater. Trans. B*, 2018, vol. 49B, pp. 3164–170.
16. Z.S. Li, M. Whitwood, S. Millman, and J.V. Boggelen: *Ironmak. Steelmak.*, 2014, vol. 41, pp. 112–20.
17. S. Kakimoto, A. Kiyose, and R. Murao: *ISIJ Int.*, 2017, vol. 57, pp. 1710–717.
18. N. Kikuchi, A. Matsui, and Y.I. Uchida: *ISIJ Int.*, 2020, vol. 60, pp. 922–29.
19. Y. Cao, Y. Xia, J. Li, and D. Fan: *Chin. J. Process Eng.*, 2020, vol. 20, pp. 1075–081.
20. E. Cheremisina, J. Schenk, L. Nocke, A. Paul, and G. Wimmer: *ISIJ Int.*, 2017, vol. 57, pp. 304–13.
21. W. Wu, Q. Gao, and B. Zhang: *J. Iron Steel Res. Int.*, 2020, vol. 27, pp. 282–94.
22. W. Wu, S. Dai, P. Wang, D. Ma, and B. Ni: *Ironmak. Steelmak.*, 2019, vol. 46, pp. 469–76.
23. D. Wang, B. Zhang, C. Hao, L. Liu, and C. Li: *Spec. Steel*, 2019, vol. 40, pp. 39–42.
24. L. Lin, J. Zeng, W. Wu, J. Wang, H. Li, C. Wang, and F. Zhang: *Chin. J. Eng.*, 2022, vol. 44, pp. 1575–584.
25. S. Dai, W. Wu, X. Zhang, and P. Wang: *China Metall.*, 2017, vol. 27, pp. 12–8.
26. V.D. Eisenhüttenleute: *Slag atlas*. Woodhead Publishing Limited, Cambridge, 1995.

Publisher's Note Springer Nature remains neutral with regard to jurisdictional claims in published maps and institutional affiliations.

Springer Nature or its licensor (e.g. a society or other partner) holds exclusive rights to this article under a publishing agreement with the author(s) or other rightsholder(s); author self-archiving of the accepted manuscript version of this article is solely governed by the terms of such publishing agreement and applicable law.